JOURNAL OF GEOPHYSICAL RESEARCH, VOL. 115, F03010, doi:10.1029/2009JF001509, 2010

Surface ice motion deviating toward the margins during speed-up events at Gornergletscher, Switzerland

S. Sugiyama,[1,2] A. Bauder,[2] P. Riesen,[2] and M. Funk[2]

Received 31 August 2009; revised 22 March 2010; accepted 30 March 2010; published 27 July 2010.

[1] High frequency ice flow measurements during speed-up events in Gornergletscher, Switzerland, revealed intriguing ice motion which has never been reported in detail before. During the summer 2005, more than a 100% flow speed increase was observed three times at four GPS stations installed across Gornergletscher. The speed-ups were accompanied by a decimeter scale surface uplift. Two of the events were triggered by intensive surface melt and rainfall, while the third one was due to the outburst of Gornersee, a glacier-dammed lake located 2 km upglacier. An interesting observation was ice motion deviating toward the side margins during the events. As the glacier accelerated, a transverse (cross glacier) velocity component was generated, turning the flow direction away from the central flow line toward the margins. When the glacier decelerated, the transverse velocity component reversed so that the ice flowed back to the azimuth of the initial flow direction. In the most significant case, the trajectory of the survey stake deviated from the original track by 0.2 m in the transverse direction. We hypothesize that the observed lateral ice motion was caused by locally elevated subglacial water pressure. When the ice sole decoupled from the bed at a part of the glacier, a point source of vertical displacement was transmitted to the surface through viscous ice. This caused the transverse as well as vertical surface motion, as observed in ground motion during magma intrusion. The hypothesis was tested with a two-dimensional ice flow model applied to the transverse glacier cross section. The model confirmed that the surface ice would move toward the margins as observed in Gornergletscher, if subglacial water pressure exceeded the ice overburden pressure over a limited part of the bed.

Citation: Sugiyama, S., A. Bauder, P. Riesen, and M. Funk (2010), Surface ice motion deviating toward the margins during speed-up events at Gornergletscher, Switzerland, *J. Geophys. Res.*, *115*, F03010, doi:10.1029/2009JF001509.

1. Introduction

[2] Glacier flow speed increases over a period of several days, referred to as 'speed-up events' in this paper, have been observed at a number of glaciers [e.g., *Iken et al.*, 1983; *Kamb and Engelhardt*, 1987; *Hooke et al.*, 1989; *Naruse et al.*, 1992; *Gudmundsson et al.*, 2000; *Mair et al.*, 2001; *Truffer et al.*, 2001; *Anderson et al.*, 2004]. Many events have been observed early in summer, but may occur throughout the ablation season. Surface flow speeds increase by more than a factor of two within a day, and peak magnitudes widely vary with the glacier and events. Speed-up events are usually triggered by an increase in water input to the subglacial drainage system, which is caused by intensive snow- and ice melt, heavy rainfall, or a sudden release of water impounded in or beside a glacier. Outburst of a glacier-dammed lake is one of these triggers, and it often causes extraordinary changes in the glacier flow regimes [e.g., *Magnússon et al.*, 2007]. The acceleration is often associated with high subglacial water pressure [*Iken and Bindschadler*, 1986; *Jansson*, 1995; *Sugiyama and Gudmundsson*, 2004]. This observation implies that basal ice motion is enhanced by water pressure, which is elevated during the adjustment of the drainage system to the water influx [*Bindschadler*, 1983; *Nienow et al.*, 1998; *Bartholomaus et al.*, 2008]. Therefore, the study of speed-up events is particularly important to furthering the understanding of the mechanism of basal ice motion and its connection to the subglacial hydraulic conditions.

[3] During the speed-up, upward glacier surface motion (so-called uplift) has been observed on many glaciers [e.g., *Iken et al.*, 1983; *Kamb and Engelhardt*, 1987]. For example, observations on Unteraargletscher showed that the surface gradually moved upward by 0.15 m within a few days when the glacier accelerated in early summer [*Iken et al.*, 1983]. The surface uplift can be explained by the separation of the glacier from the bed due to elevated water pressure. Water cavity formation at the lee side of bedrock bumps is one of

[1] Institute of Low Temperature Science, Hokkaido University, Sapporo, Japan.
[2] Laboratory of Hydraulics, Hydrology and Glaciology, ETH Zurich, Zurich, Switzerland.

0148-0227/10/2009JF001509

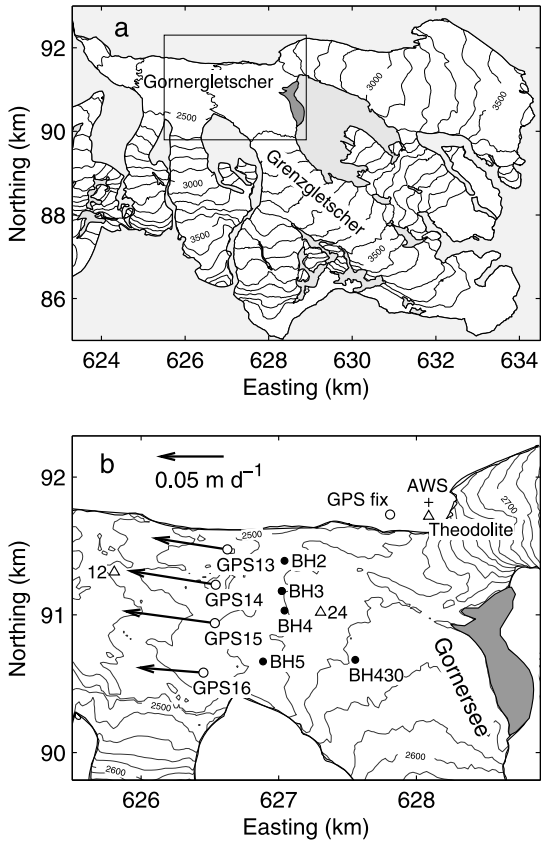

Figure 1. (a) Map of Gornergletscher and Grenzgletscher with the study site indicated by the box and the Gornersee indicated by the gray hatch. Surface contour spacing is 100 m. Coordinates are in the official Swiss coordinate system. (b) Locations of the GPS stations (open circles), theodolite and reflectors (triangle), boreholes (solid circles), and automatic weather station (AWS, plus sign). The vectors are horizontal flow velocities measured from May 15 to August 25, 2005. Surface contour spacing is 20 m.

the mechanisms proposed for the basal separation [e.g., *Röthlisberger and Iken*, 1981]. Although the occurrence of basal separation is likely during a high velocity period, the vertical surface motion may not be solely attributed to a separation of the glacier from its bed. Vertical strain integrated over the ice thickness is an important component of the vertical motion, and temporal variation in the strain rate is significant under changing subglacial and englacial stress conditions [*Gudmundsson*, 2002; *Sugiyama and Gudmundsson*, 2003]. Sliding along an inclined bed may contribute to vertical surface motion as well [*Hooke et al.*, 1989; *Mair et al.*, 2002; *Anderson et al.*, 2004], making it more difficult to interpret surface observations. To fully understand the cause of the surface uplift, it is crucial to measure flow speed, water pressure, strain regimes, and bed geometry, and compare them with the details of vertical surface motion. High frequency Global Positioning System (GPS) survey techniques, and water pressure and strain measurements in boreholes provide a possibility to collect data for an accurate understanding of the uplift mechanisms.

[4] During summer 2005, we installed four GPS receivers on Gornergletscher to measure short-term ice flow variations. The primary objective of the field campaign was to study a glacier-dammed lake outburst which was expected to occur in the summer. We aligned the GPS receivers across the glacier to detect the location of the lake water drainage from the changes in the ice motion. We expected that the magnitude of the acceleration and uplift would be greater above the drainage path than elsewhere. When the lake drained, in addition to the expected speed-up and uplift, we observed intriguing ice motion toward the glacier margins. The transverse motions coincided with the uplift and they were distributed systematically across the glacier. These details are revealed for the first time in this study as a result of the multiple GPS installations across the glacier. Similar ice motion was recognized in two other speed-up events earlier in the melt season.

[5] In this paper we report the details of the three speed-up events that occurred in Gornergletscher in summer 2005, with special focus on the surface ice motion in transverse and vertical directions. The observed ice motion can be reproduced with a two-dimensional numerical ice flow model by assuming that the subglacial water pressure exceeds the ice overburden pressure over a limited part of the glacier. Thus, we propose that the glacier decouples from the bed at a pressurized subglacial drainage path, resulting in the upward and transverse motion on the surface. Our field data reveal a peculiar dynamic behavior during a speed-up event, and the numerical modeling demonstrates a possible procedure to assess basal ice motion and hydraulic conditions from surface observations.

2. Field Measurements

2.1. Study Site

[6] Gornergletscher is the second largest glacier system in the Swiss Alps with a surface area of 38 km^2 for major tributaries and 53 km^2 for the whole system [*Bauder et al.*, 2007]. The upper part of the 12-km long mainstream is named Grenzgletscher; it merges with Gornergletscher at about 5 km from the common terminus of the glacier system (Figure 1a). Due to the thinning of the upper part of Gornergletscher, ice flux and flow regime in the confluence area are dominated by the flow from Grenzgletscher [*Sugiyama et al.*, 2007]. Borehole temperature and ice radar measurements showed the existence of a cold ice body in the confluence area at temperatures down to 2.5 K below the pressure melting point [*Ryser*, 2008; *Eisen et al.*, 2009]. The cold ice occupies the central part of the glacier from the surface to more than 50% of the ice thickness, and this cold layer is underlain by a temperate basal layer. The lateral and vertical extent of the cold ice decreases downglacier.

[7] One of the characteristic features of Gornergletscher is the formation of a glacier-dammed lake, Gornersee, at the eastern margin of the confluence (Figure 1). Gornersee forms every spring as water from snow- and ice melt collects, and then drains away that same summer, releasing several million cubic meters of water. We studied the outburst events from 2004 to 2008 by conducting detailed field observations [*Huss et al.*, 2007; *Sugiyama et al.*, 2007, 2008; *Walter et al.*, 2008; *Werder et al.*, 2009; *Werder and Funk*, 2009]. Our observations revealed that the triggering and drainage mechanisms of the outburst vary from year to year. However, significant changes in the ice flow regime, e.g., acceleration,

direction change, uplift, accompanied by an increase in subglacial water pressure, have been observed in each of the events.

[8] The 2005 field measurements began in April by installing GPS receivers and an automatic weather station, followed by a borehole drilling campaign in June. The ice flow and water pressure data presented in this paper were obtained at about 1–2 km downglacier from Gornersee. The glacier surface of this region became snow-free in late May. Lake water level was measured with a pressure sensor installed near the deepest point in Gornersee. The lake level dropped on June 11 when the lake water volume was less than a third of the full capacity. It was difficult to determine the true onset of the outburst as the water had begun to leak about a week before the lake level began to decrease. According to the lake discharge, about 80% of the lake water drained during the three days from June 12 to 14 [*Huss et al.*, 2007].

2.2. Method

2.2.1. Ice Flow Measurements

[9] Surface ice motion was measured either with GPS or a theodolite by surveying the three-dimensional coordinates of aluminum stakes installed on the glacier. The stakes were drilled several meters deep into the ice and stake length above the surface was maintained to be less than 2 m in order to reduce the influence of wind on survey accuracy. The locations of the stakes used for this study are shown in Figure 1b together with summer flow vectors obtained for the period from May 15 to August 25, 2005.

[10] Four stakes named GPS13-16 were installed across the glacier at distances of 250 to 350 m from each other (Figure 1b). From May to September 2005, these stakes were surveyed by GPS (Leica System 500) at intervals of 3 hours. The L1 and L2 GPS phase signals were recorded with a GPS antenna mounted on the top of the stake and post-processed in a static mode using Leica SKI-Pro software with reference data recorded by a fixed GPS station on bedrock at the northern glacier flank (Figure 1b). The accuracy of the positioning was estimated from winter measurements at the study site (December 1–31, 2003, n = 121). Assuming a constant flow speed and direction during the winter measurement period, standard deviations from expected stake locations were 3.4 and 4.2 mm in the horizontal and vertical directions, respectively. From May 12 to June 4, stake GPS16 was measured by a theodolite instead of GPS using the technique described below.

[11] Stakes 12 and 24 were equipped with reflectors on the top to be surveyed with a theodolite (Leica TCA1800) installed on the bedrock at the northern flank (Figure 1b). The theodolite was automatically operated every hour from May to September 2005, unless the operation was interrupted by weather conditions or equipment failure. The data obtained were corrected by surveying reference reflectors fixed on bedrock in the vicinity of the margin. The standard deviation of the positioning is about 5–10 millimeters, depending on the distance from the theodolite to the reflectors [*Sugiyama et al.*, 2008].

[12] The surveyed coordinates were smoothed using a Gaussian filter to calculate horizontal flow speed and strain rate. The smoothing bandwidth was fixed in the range of 0.125–0.75 days depending on the magnitude of the positioning errors (GPS or theodolite) and the smoothness required for the calculations (speed or strain rate).

2.2.2. Water Pressure Measurements

[13] Subglacial water pressure in borehole BH430 (Figure 1b) has been measured since the summer 2004. Pressure measurements in four additional boreholes BH2–5 (Figure 1b) began in early June 2005, shortly before the outburst event. These boreholes were drilled down to the bed by a hot-water drilling system. According to the length of the hose used for the drilling, the ice thicknesses at the drilling sites BH430, and BH2–5 were 430, 251, 354, 384, and 227 m, respectively. These values are in good agreement with the thicknesses obtained by radio echo soundings [*Sugiyama et al.*, 2008]. Errors due to the stretching of the hose are about 2–3% of the ice thickness. The thickness at BH430 is not as accurate as the others because of surface melting and vertical straining after the drilling in 2004. The water pressure was measured near the bottom of the boreholes with vibrating wire pressure transducers (Geokon Model 4500) and recorded with data loggers (Campbell CR10X) at intervals of 10 min. The accuracy of the measurement was equivalent to a change in water level of ±0.35 m. In borehole BH430, the water level may have an error of up to ±10 m because of the uncertainty in the distance between the bed and the sensor.

2.2.3. Meteorological Measurements

[14] A meteorological station was established on the glacier flank near the theodolite at 2600 m a.s.l. (Figure 1b). Air temperature and precipitation were measured from April 2005 at 30 min intervals with a ventilated thermistor sensor (Vaisala T107) and with a tipping bucket rain gauge (Joss-Tognini), respectively.

3. Results

3.1. Speed-Up Events

[15] Three speed-up events were observed during the study period, twice in May and once in June. At each event, flow speed increase and surface uplift occurred for about 5 days (Figures 2a and 2b). We refer to these speed-up events as Event 1 (May 20 0000 h–May 24 1200 h), Event 2 (May 26 0000 h–May 31 1200 h), and Event 3 (June 11 0000 h–June 16 1200 h).

[16] Event 1 began on May 20 when the air temperature rose after a cold period (Figure 2c). The horizontal surface speed increased with weak diurnal signals, and it peaked on May 22 about a day after heavy precipitation (Figures 2a and 2c). The peak speeds were about three times greater than those before the event. GPS13–15 recorded a surface uplift of 0.05–0.1 m during the period of acceleration (Figure 2b). The horizontal speed decreased to the pre-event level when the air temperature dropped on May 24, whereas the surface remained elevated at a higher level. The water level slightly dropped over the course of the event, but no significant fluctuation was observed (Figure 2d).

[17] Event 2 was characterized by strong diurnal variations in the flow speed (Figure 2a). The diurnal signals were also present in the vertical displacement (Figure 2b). The flow speed increased and the ice surface moved upward in the afternoon, whereas the speed decreased and the surface moved downward in the morning. The flow speeds at GPS13–16 peaked on May 28 and they were about three

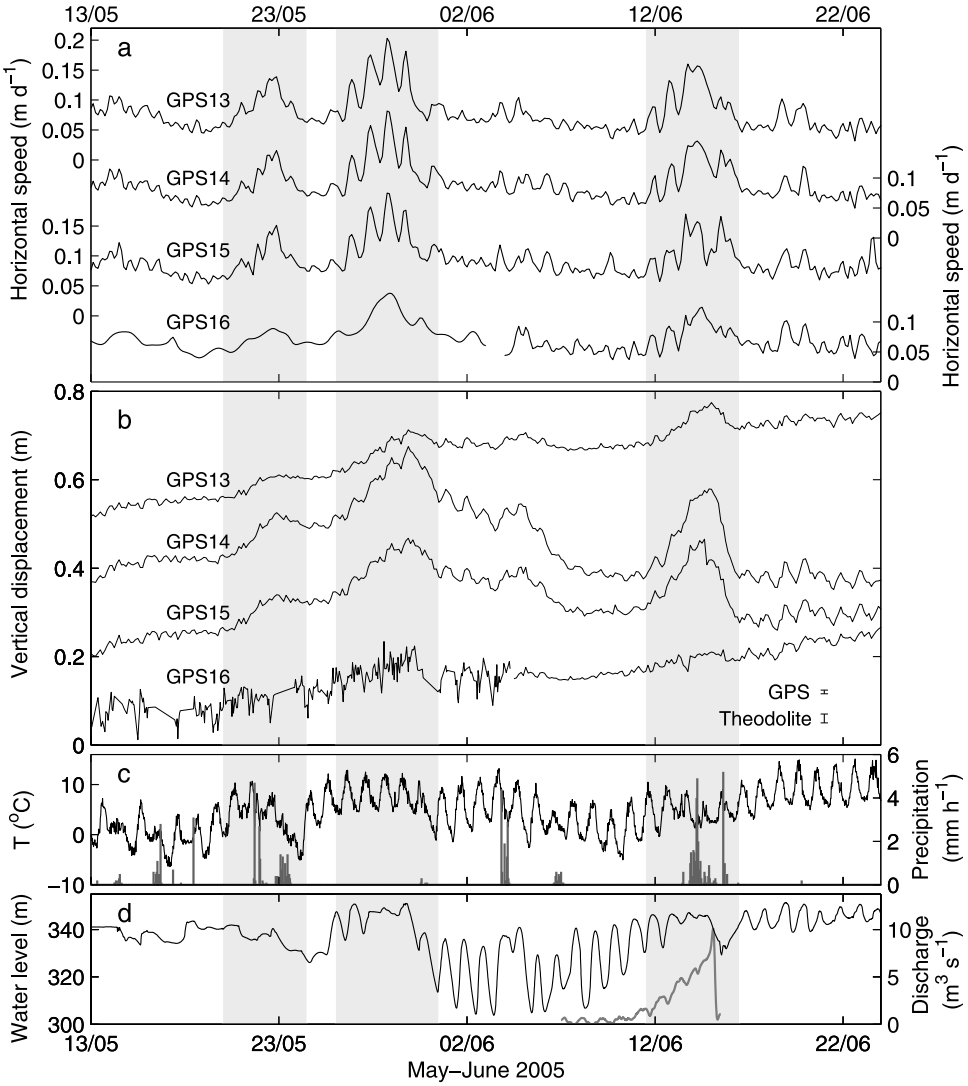

Figure 2. Time series of (a) horizontal flow speed, (b) vertical displacement, (c) air temperature (line) and precipitation (column), and (d) borehole water level in BH430 (black) and discharge from Gornersee (gray bold). The gray bands indicate the periods of speed-up events. The stake GPS16 was surveyed by a theodolite until June 4. The GPS and theodolite data used for the horizontal speed calculations were filtered with bandwidths of 0.125 and 0.375 d, respectively. The error bars in Figure 2b correspond to the standard deviations of the GPS (±4.2 mm) and theodolite (±10 mm) measurements. The lake discharge was derived from the lake level and modeled meltwater input [*Huss et al.*, 2007].

times greater than the speeds before the event. The magnitude of the uplift was greater at the glacier center, reaching 0.2 m at GPS14. After this event, the generally upward vertical motion since the beginning of the measurements turned into a downward trend at GPS14 and GPS15. This observation contrasts to GPS13 and GPS16, which showed upward motion trend throughout the measurement period. The air temperature showed steady diurnal variations at a relatively high level (Figure 2c) suggesting a large amount of meltwater production during the daytime. The borehole water level began to show diurnal signals at the onset of the event (Figure 2d). The pressure dropped at the end of the event, coincided with the beginning of clear diurnal oscillations with an amplitude of about 20 m.

[18] Event 3 was caused by the outburst of Gornersee. The flow speeds at GPS13–16 increased with diurnal variations and reached their maxima on June 14 (Figure 2a), one day before the lake discharge peaked (Figure 2d). The magnitude of the uplift at GPS14 and GPS15 was about 0.2 m, while no significant vertical displacement was observed at GPS16 (Figure 2b). The large uplift at GPS14 and GPS15 was followed by a similar magnitude of downward motion. A substantial amount of precipitation (26 mm in total) was recorded during this period (Figure 2c). The borehole water level had risen since several days before the onset of the speed-up, and the high pressure condition lasted longer after the event (Figure 2d).

3.2. Ice Motion Deviating Toward the Margins

[19] During the speed-up events, anomalous ice motion was observed. The trajectory of the stake motion at GPS13 indicates that the ice moved toward the right margin

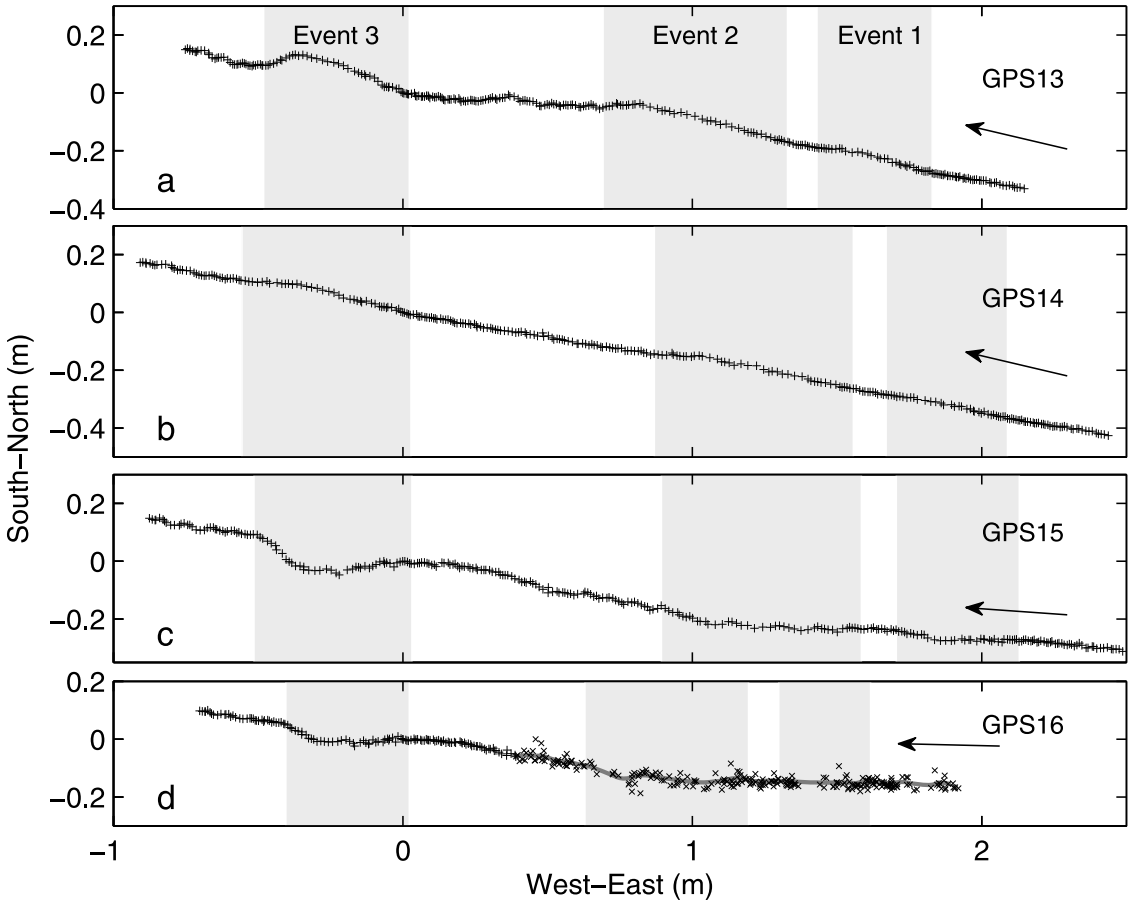

Figure 3. Plan view of the stake motion measured with GPS (plus signs) and theodolite (crosses) at (a) GPS13, (b) GPS14, (c) GPS15, and (d) GPS16 from May 15 to June 21, 2005. The flow directions are from right to left. The gray bands indicate the periods of speed-up events. The gray line for GPS16 is drawn by filtering the theodolite data with bandwidths of 0.375 d.

(looking down the glacier) during the first half of the events and switched back to the original track during the second half (Figure 3a). In other words, the transverse (cross glacier) velocity component was generated at the onset of the event, and then the transverse velocity became negative until it returned to zero after the event. Among the three events, the deviation from the original track was greatest in Event 3, but smaller deviations were also recognized in the other two events. Similar flow changes were observed at GPS14 (Figure 3b), although the magnitude was smaller than that at GPS13. At GPS15 and GPS16, the directions of the flow changes were opposite to those at GPS13 and GPS14, i.e., toward the left margin (Figures 3c and 3d). It was clearly observed in Event 3 that the directions of the deviation were to the right in the right half of the glacier and to the left in the left half. In the remainder of this paper, we refer to these ice movements in the transverse directions as 'marginward ice motion'.

[20] The marginward ice motion coincided not only with the speed-up, but also with the surface uplift. Figure 4 shows the trajectories of the stake motion in the vertical and cross glacier (south-north) directions after removing the linear trends between the onset and the end of the events. The detrended trajectories indicate correlations between the transverse ice motion and uplift. The maximum displacement in the transverse and vertical directions occurred at approximately the same time. The trajectories exhibit hysteresis, but the stake motion basically follows the lines pointing to the maximum displacements, as represented by GPS13 during Events 2 and 3 (Figures 4b and 4c). Thus, the transverse displacement was linearly correlated to the vertical displacement. The direction of the ice motion at each stake was similar in the three events. For example, the transverse ice motion at GPS15 was toward the south, and its magnitude was about half of the vertical displacement in each event. Therefore, the proportion of the transverse to the vertical velocity was approximately the same in the three events, and the only difference was the magnitude of the displacement.

[21] The marginward ice motion gave rise to significant changes in the transverse strain rate regime. Strain rates were computed between the survey stakes (GPS13–14, GPS14–15, and GPS15–16) and the right margin (margin–GPS13), using the south-north displacements of the stakes and assuming no lateral ice movement at the margin where ice is confined by the sidewall (Figure 5a). The strain rates at GPS13–14 and GPS14–15 were well correlated throughout the study period. During the speed-up events, the strain rates were tensile (positive) in the first half of the events, and then reversed to compressive (negative) in the second half.

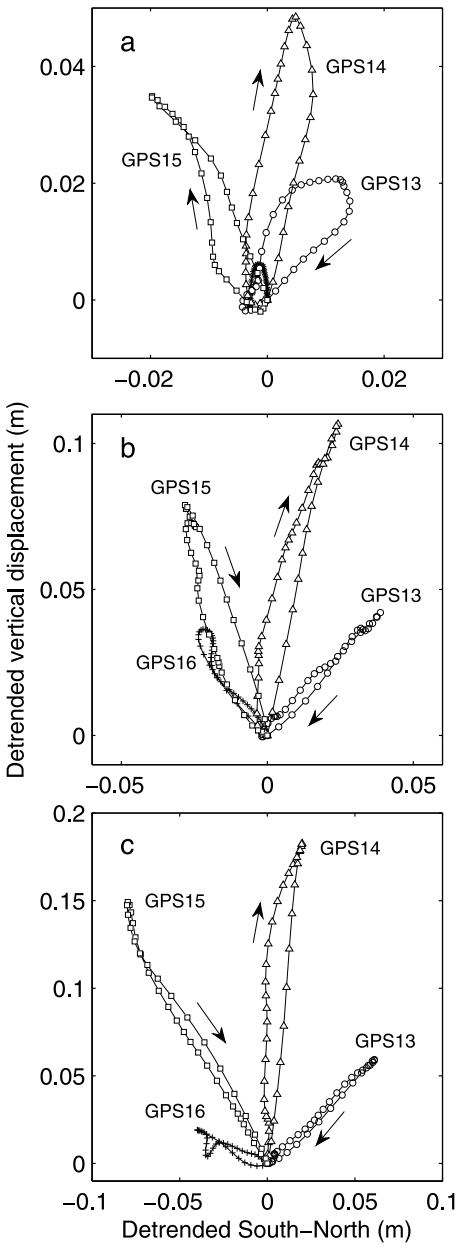

Figure 4. Surface ice motion projected on the south-north vertical plane at GPS13 (open circles), GPS14 (triangles), GPS15 (squares), and GPS16 (plus signs) during (a) Event 1, (b) Event 2, and (c) Event 3. Linear trends between the onset and the end of the events were removed from the motion. The GPS and theodolite data were filtered with bandwidths of 0.25 and 0.75 d, respectively.

Superimposed on these changes were diurnal variations, which showed tensile strain rates in the afternoon and compressive strain rates in the morning. These variations in the central part of the glacier were inversely correlated to those in the marginal regions (margin–GPS13 and GPS15–16). Therefore, the observed changes in the transverse strain rate were as follows. During the period of velocity increase (i.e., first half of the events or afternoon), the glacier ice was stretched in the central part and compressed in the marginal regions. The strain rates were reversed when the ice decelerated (second half of the events or morning). The spatial and temporal variations shown in Figure 5b clearly display such trends during the study period.

4. Interpretation of the Field Data

4.1. Cause of the Speed-Up Events

[22] The climatic data and subglacial water pressure indicated that the three speed-up events were related to increased water input to the glacier bed. Event 1 was caused by the combination of temperature increase and rainfall as observed in Figure 2c. The glacier reacted to them in a sensitive way, probably because the hydraulic system was undeveloped at this time of the season. The uplift during Event 1 was smaller than those during other events (Figure 2b), which implies that this event was triggered by a relatively small amount of water input.

[23] Event 2 was a typical speed-up event in the early melt season triggered by a period with high temperature. It is likely that a large amount of meltwater drained along the glacier bed and increased the subglacial water pressure as recorded in the borehole water level (Figure 2d). The pressure began to fluctuate diurnally after this event, suggesting that the subglacial drainage became more efficient by opening drainage conduits. The surface snow in the study site disappeared approximately at this time of the season, which has been observed to coincide with transformation from an inefficient distributed drainage system into a conduit system [*Nienow et al.*, 1998].

[24] It is evident that Event 3 was triggered by the outburst of Gornersee. Its magnitude and rate of uplift were greater than those during the other two events, as expected from the sudden release of a large amount of lake water to the glacier bed (Figure 2d). During the outburst event, temporary water storage in the glacier system attained 54% of the total lake water [*Huss et al.*, 2007].

[25] These events showed various interesting responses of the glacier dynamics to the changes in the subglacial hydraulic conditions. Nevertheless, here we focus on the marginward ice motion.

4.2. Mechanism of the Marginward Ice Motion

[26] The marginward ice motion in Gornergletscher is not unique to the observations made in 2005. Field measurements in Gornergletscher were repeated from 2006 to 2008, and essentially the same ice motion was observed during lake outbursts by means of stake measurements and interferometric radar technique [*Riesen et al.*, 2009]. Similar flow direction changes were recognized in Hansbreen during a speed-up event [*Vieli et al.*, 2004], although it was not possible to determine if the flow change was systematically distributed across the glacier as the survey points were limited. Direction changes during summer acceleration are reported in Greenland as well [*Zwally et al.*, 2002]. These observations suggest that such ice motion commonly occurs in other glaciers. The marginward ice motion was clearly related to the speed up and surface up lift, which were caused by changes in the subglacial conditions. Based on the magnitude and the direction of the transverse ice motion at GPS13–16 together with their close relationship with the uplift, we discuss a mechanism which connects basal perturbation to the marginward ice motion.

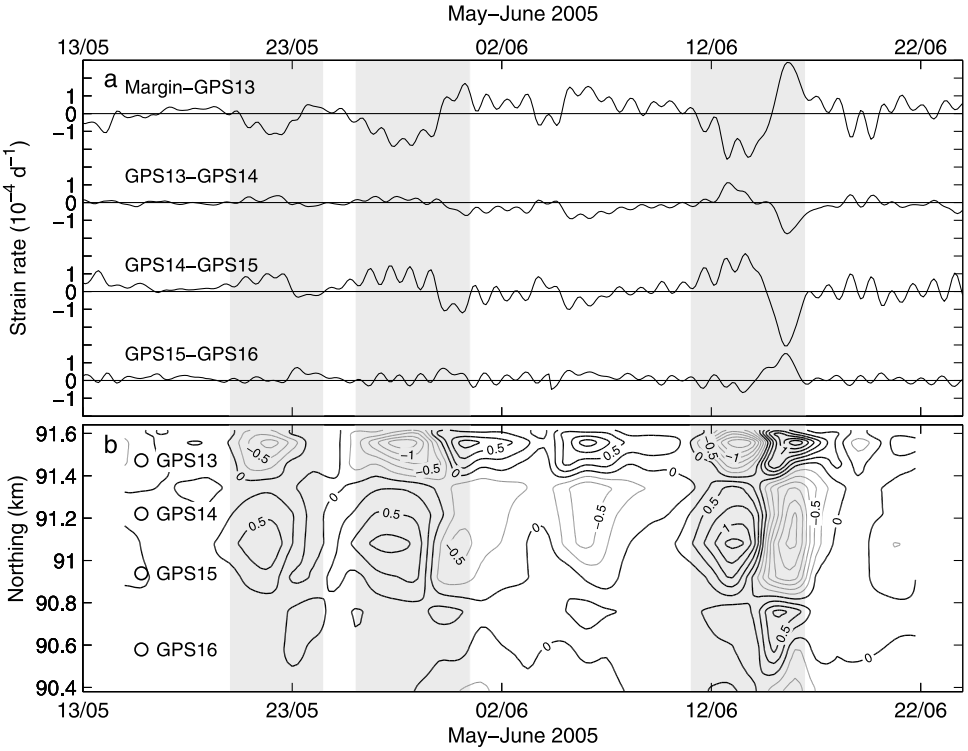

Figure 5. (a) Time series of transverse strain rate and (b) its distribution across the glacier. Intervals of the contour lines are 0.25×10^{-4} d^{-1} with gray lines for negative (compressive) strain rate. The gray bands indicate the periods of speed-up events. The GPS and theodolite data used for the strain rate calculations were filtered with bandwidths of 0.25 and 0.75 d, respectively.

[27] The mean flow vectors during the first half of Event 3 (June 11 0000 h–June 14 0000 h) are projected on the vertical glacier cross section along the GPS stations (Figure 6). The linear trend during the event (June 11 0000 h–June 16 0000 h) is subtracted from the stake displacement. As a mechanism of this transverse and upward motion, we propose basal separation beneath the central part of the glacier caused by locally elevated subglacial water pressure. When the glacier bed is pressurized above the overburden pressure, the glacier sole is decoupled from the bed. If we assume that the basal separation is spatially limited in the central part and the ice in the remaining regions is still in contact with the bed, the surface moves vertically upward above the decoupled zone while it moves up and marginward at off-center locations. Such surface motion is expected when a point source of vertical motion propagates through a viscous medium, and can be understood by analogy with vertical and horizontal ground motion due to the intrusion of magma [e.g., *Mogi*, 1958; *Walsh and Decker*, 1971]. It is most likely that the reversal in the transverse ice motion occurred when the water pressure dropped and the space created by the basal separation collapsed owing to the ice pressure.

[28] The ice surface motion shown in Figure 6 can be expected when a subglacial drainage or a highly pressurized zone is located approximately beneath GPS14. Flow speed and surface elevation before, during, and after Event 3 provide insights into the location of subglacial drainage due to the lake outburst. The flow speed profile across the glacier shows that the right side of the glacier was more accelerated during the outburst (Figure 7a). The surface uplift was also greater in the right side and the maximum elevation change was observed at GPS14 (Figure 7b). The surface lowering after the event at GPS14 and GPS15 implies a closure of the drainage conduit underneath. These observations indicate that the lake water was routed through the right side of the glacier and the bed became more pressurized in that region, resulting in enhanced basal ice motion and separation. A hydraulic potential analysis also suggested the location of the main drainage channel in the region beneath GPS14–15 [*Werder and Funk*, 2009]. Similar flow speed variations across a glacier have been used to

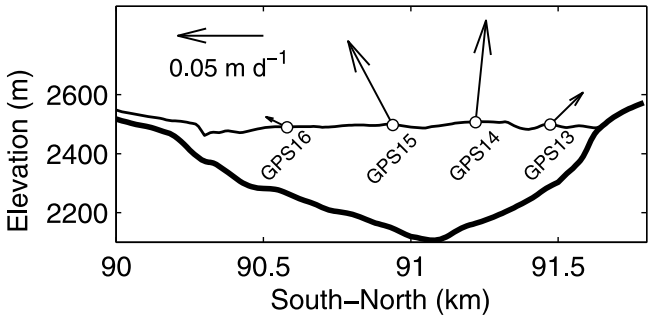

Figure 6. Vertical cross section of Gornergletscher along the GPS stations. The mean flow vectors for the first half of Event 3 (June 11 0000 h–June 14 0000 h) are projected on the vertical plane. Linear trends between the onset (June 11 0000 h) and the end (June 16 0000 h) of Event 3 are subtracted from the flow vectors.

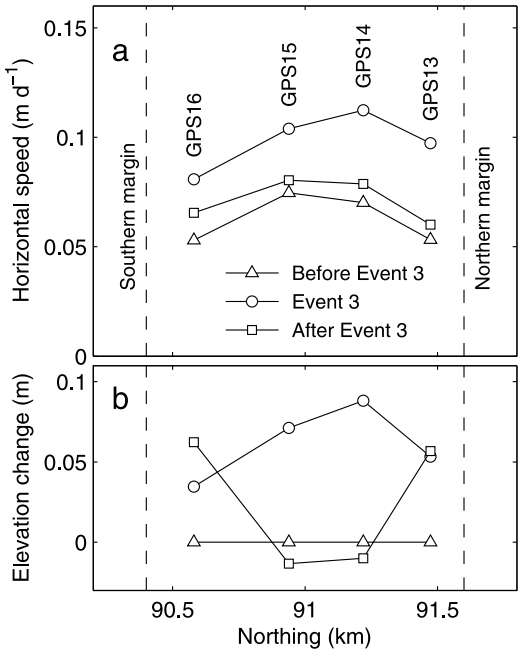

Figure 7. (a) The mean horizontal flow speed and (b) mean surface elevation before (June 6 1200 h–June 11 1200 h), during (June 11 1200 h–June 16 1200 h), and after Event 3 (June 16 1200 h–June 21 1200 h). The elevation is measured relative to the surface before Event 3.

estimate basal stress distributions in Haut Glacier d'Arolla [*Hubbard et al.*, 1998; *Nienow et al.*, 2005] and Black Rapids Glacier [*Amundson et al.*, 2006]. These studies attributed the changes in transverse flow speed profiles to a localized subglacial drainage pattern, as we assume here.

[29] The borehole water levels in BH2–5 provide more direct information on the location of the subglacial drainage path (Figure 8). The water level was elevated in BH3 during Event 3, and it began to show clear diurnal variations after the event. Similar water level variations were observed in BH4. In contrast to BH3 and BH4, the boreholes near the margins, BH2 and BH5, filled up with water and showed no significant variations during the event. Small fluctuations after Event 3 at BH2 may indicate poor connection to a drainage system, but BH5 showed no evidence of connection. These observations and the borehole locations imply that the flow path of the lake water was located in the region beneath GPS13–15, resulting in greater acceleration and uplift in the right side of the glacier. Surface ice motion as a response to locally elevated subglacial water pressure is discussed more in detail in the next section by using a numerical ice flow model.

[30] The water levels in BH3 and BH4 were nearly equal to the overburden levels during Event 3 (Figure 8). This observation supports our assumption that basal separation occurred because of water pressure exceeding the ice overburden. Another mechanism of basal separation is water cavity formation due to ice sliding over bedrock bumps [e.g., *Röthlisberger and Iken*, 1981]. Growth of cavities at spatially limited area of glacier bed may cause similar vertical and transverse ice motion as we discussed above. In this case, the rate of surface uplift should be related to the basal sliding speed. Our data show that the uplift rates in Event 3 are greater than those in Event 2, whereas the surface speeds in Event 3 are smaller than those in Event 2 (Figures 2a and 2b). Thus, the observed ice motion cannot be explained by basal separation due to cavity formation. Basal sliding along an up-glacier inclined bed slope also causes vertical ice motion [*Hooke et al.*, 1989]. *Anderson et al.* [2004] found a similar upward slope (proportion of horizontal to vertical displacement) in surface ice trajectories during two speed-up events in Bench Glacier, Alaska. They suggested sliding over stoss slopes of bedrock bumps as an interpretation of the vertical surface motion which was consistent during each event. In Gornergletscher, upward slopes of the trajectories projected on a vertical plane along ice motion are not consistent during each event (Figure 9). For example, the slopes at GPS13–15 during Event 3 are greater than those in Event 2. Because of the reasons above, we hypothesize basal separation due to pressurized water as the key mechanism of the marginward ice motion.

4.3. Strain Rate Regime

[31] The transverse strain rate at the glacier center became tensile during the first half of the events, and turned to compressive during the second half (Figure 5). These strain rates are one to two orders of magnitude greater than the mean transverse strain rate derived from the summer flow velocities at GPS13 and GPS16 (5.7×10^{-6} d^{-1} for the period from May 15 to August 25, 2005). Thus, the observed changes cannot be explained by sudden acceleration or deceleration of ice along a narrowing or widening valley.

[32] The transverse extension and compression could be caused by longitudinal compression and extension, respectively. Such changes in the strain rate regime may have been generated by a wave of accelerated ice motion propagating

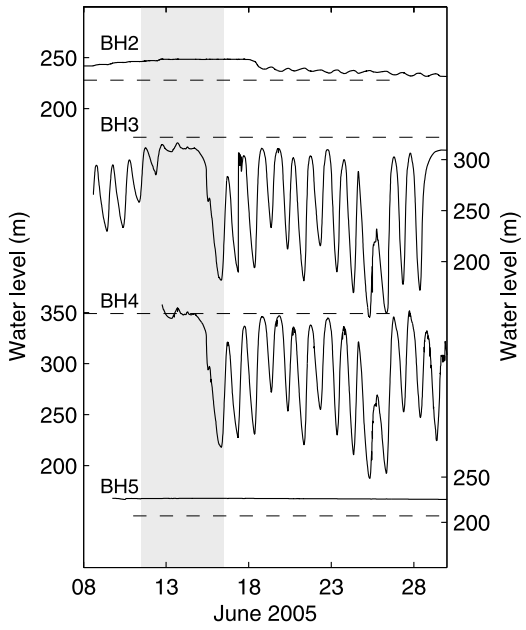

Figure 8. Time series of water level in the boreholes BH2–5. The ice overburden level at each borehole site is shown by the dashed line. The gray band indicates the period of Event 3.

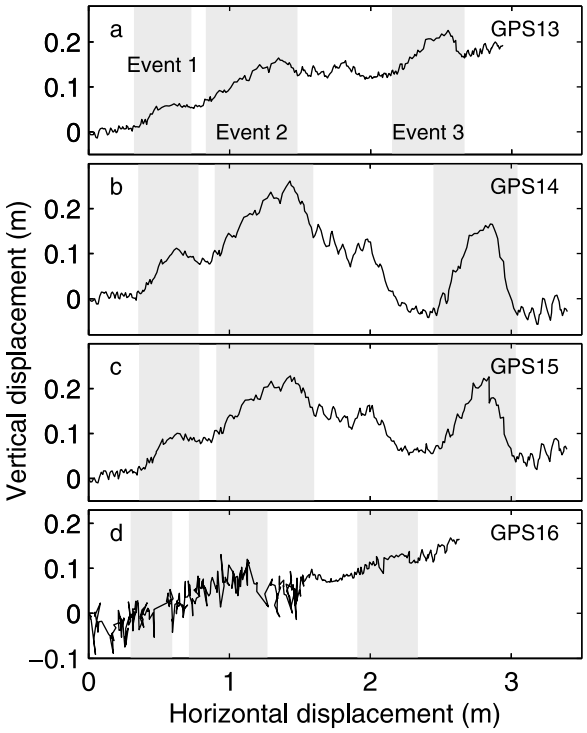

Figure 9. Surface ice motion projected on a vertical plane parallel to the ice motion at (a) GPS13, (b) GPS14, (c) GPS15, and (d) GPS16 from May 15 to June 21, 2005. The gray bands indicate the periods of speed-up events.

down the glacier. Downglacier propagation of accelerated motion has been observed in other glaciers [*Kamb and Engelhardt*, 1987; *Gudmundsson*, 2002; *Vieli et al.*, 2004], and used to interpret short-term variations in longitudinal and vertical strain rates [*Raymond and Malone*, 1986; *Gudmundsson*, 2002]. Although changes in the transverse strain rate were not observed in these studies, longitudinal strain rate variations during the events should be analyzed as a possible cause of the marginward ice motion.

[33] Longitudinal strain rate was computed for the period of Event 3 from the horizontal flow speed measured by the theodolite at stakes 12 and 24. The result was compared with the transverse strain rate from the GPS data to assess whether the transverse extension and compression were counteracted by longitudinal compression and extension, respectively (Figure 10). The flow speed at stake 24 was greater than that at stake 12, except for a short period in the middle of the event (Figure 10a). From June 13 to 14, the speed at stake 12 exceeded that at stake 24, resulting in the reversal of the longitudinal strain rate from compressive to tensile (Figure 10b). The strain rate then became compressive toward the end of the event as the speed decreased at stake 12. If this strain rate reversal was the cause of the marginward ice motion, an inverse correlation should be observed between the longitudinal and transverse strain rates. However, the observed strain rates do not support this hypothesis (Figure 10c). Moreover, the transverse strain rate is one order of magnitude greater than the longitudinal strain rate. Therefore, it is not likely that the marginward ice motion was caused by longitudinal compression and extension.

5. Numerical Experiments

[34] To test the hypothesis that the marginward ice motion was generated by locally elevated subglacial water pressure, numerical experiments were carried out by applying a two-dimensional ice flow model to the transverse glacier cross section. The aim of the experiments was to compute vertical and transverse velocity fields in the cross section to investigate whether the model reproduces marginward surface motion as a response to a subglacial water pressure being locally higher than the ice overburden pressure.

5.1. Model

[35] The cross section of Gornergletscher along the GPS stations was approximated with a quadratic function for the bed and a flat surface (Figure 11a). By taking y- and z-coordinates in the transverse and vertical directions, momentum and mass balance equations in the y-z plane are

$$\frac{\partial \sigma_{yy}}{\partial y} + \frac{\partial \sigma_{yz}}{\partial z} = 0, \tag{1}$$

$$\frac{\partial \sigma_{zy}}{\partial y} + \frac{\partial \sigma_{zz}}{\partial z} = \rho g, \tag{2}$$

and

$$\frac{\partial u_y}{\partial y} + \frac{\partial u_z}{\partial z} = 0, \tag{3}$$

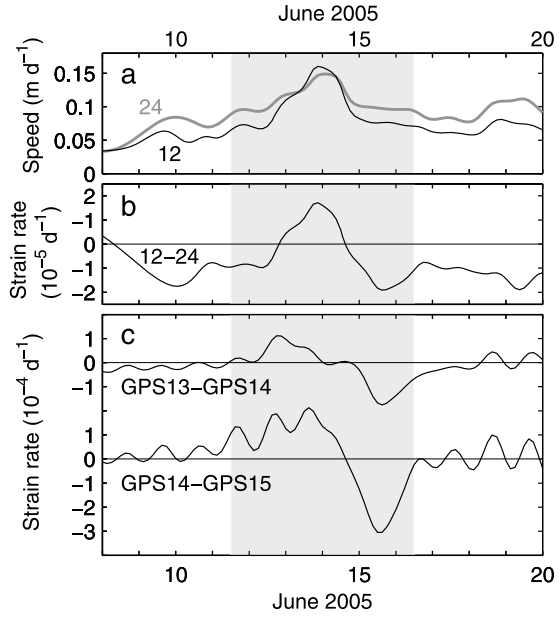

Figure 10. (a) Time series of horizontal flow speed at stakes 12 (black) and 24 (gray bold), (b) longitudinal strain rate at stakes 12–24, and (c) transverse strain rates at GPS13–14 and GPS14–15. The GPS and theodolite data were filtered with bandwidths of 0.25 and 0.375 d, respectively. The gray band indicates the period of Event 3.

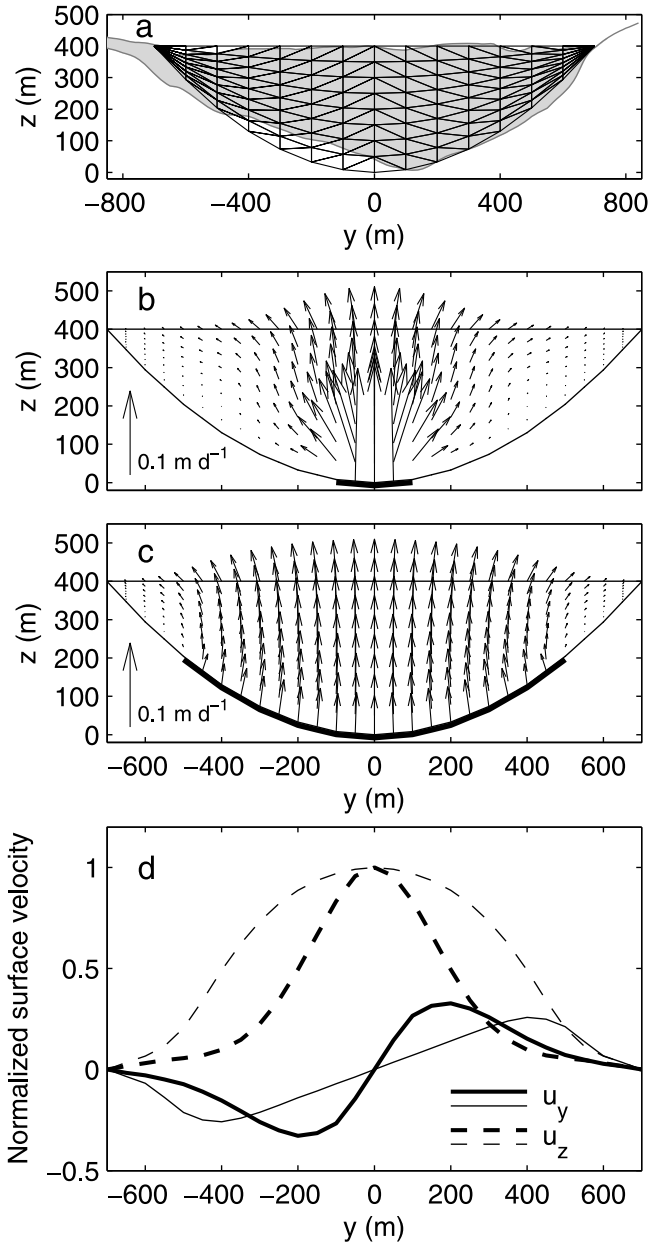

Figure 11. (a) Vertical cross section of Gornergletscher along the GPS stations GPS13–16 (looking downglacier) and a finite element mesh used for the numerical experiments. Flow vectors computed by (b) Experiment 1 and (c) Experiment 2. The bold lines at the glacier bed indicate the locations of the pressurized zones. (d) Horizontal (solid) and vertical (dashed) surface velocities in Experiment 1 (bold) and Experiment 2 (thin). The velocities in Figure 11d are normalized with the maximum vertical velocities.

where σ_{ij} are full stresses, $\rho = 910$ kg m^{-3} is the density of ice, $g = 9.81$ m s^{-2} is the gravitational acceleration and u_y and u_z are transverse and vertical velocities. The constitutive equation is given by Glen's flow law [*Glen*, 1955],

$$\dot{\varepsilon}_{ij} = A\tau_e^{n-1}\tau_{ij}, \tag{4}$$

where $\dot{\varepsilon}_{ij}$ and τ_{ij} are the components of the strain rate and deviatoric stress tensors, respectively, and τ_e is the effective stress. We took $n = 3$ for the flow-law exponent and $A = 75$ MPa^{-3} a^{-1} as a value of the rate factor for a temperate glacier [*Gudmundsson*, 1999]. In Gornergletscher, the extent of the cold ice in the modeled cross section was estimated as 300 m wide and 100–200 m thick [*Ryser*, 2008; *Eisen et al.*, 2009]. For simplicity of the model, the influence of the cold layer on A was not considered here.

[36] Equations (1)–(4) were solved for u_y and u_z with the finite element method. The code was originally developed for longitudinal ice flow modeling [*Sugiyama et al.*, 2003] and tested in the benchmark experiments for higher-order and full-Stokes ice sheet models (ISMIP-HOM) [*Pattyn et al.*, 2008]. The nonlinear ice rheology was taken into account by computing the effective stress in an iterative way until the velocity solution converged. Furthermore, the effect of the ice flow downglacier was included by solving the momentum balance along the flow line (x-direction),

$$\frac{\partial \sigma_{xy}}{\partial y} + \frac{\partial \sigma_{xz}}{\partial z} = \rho g \sin\theta. \tag{5}$$

The surface slope $\sin\theta = 0.04$ was taken from the map of Gornergletscher with a length scale of ice thickness. The shear stresses σ_{xy} and σ_{xz} obtained from equations (4) and (5) were used to compute the effective stress τ_e. The effective stress was updated by iterating the two partial differential equation systems (1)–(4) and (4)–(5) until the velocity field (u_y, u_z) converged.

[37] The modeled domain was discretized with 224 triangular quadratic elements as shown in Figure 11a. Spatial resolutions at the glacier center were 50 and 25 m in the horizontal and vertical directions, respectively. The stress-free boundary condition was imposed on the glacier surface. The bottom boundary nodes were fixed ($u_y = u_z = 0$) except for those located in a central region defined by $y_0 < y < y_1$ (pressurized zone). For the pressurized zone, instead of the fixed boundary condition, a stress boundary condition was imposed along the glacier sole:

$$n_y\sigma_{yy} + n_z\sigma_{zy} = -n_y p_w(y) \tag{6}$$

$$n_y\sigma_{yz} + n_z\sigma_{zz} = -n_z p_w(y). \tag{7}$$

The normal vector $\mathbf{n} = (n_y, n_z)$ is pointing outward from the glacier sole, and the subglacial water pressure $p_w(y)$ is given as

$$p_w(y) = \alpha p_i(y), \tag{8}$$

where p_i is the ice overburden pressure and the constant α was prescribed so that the magnitude of the vertical velocity at the glacier surface became similar to the observation in Gornergletscher. We assumed that the water pressure was greater than the ice overburden pressure ($\alpha > 1$) in the pressurized zone, which led to basal separation and surface uplift.

5.2. Results and Discussion

[38] Figure 11b shows the flow vectors obtained for a 200-m wide pressurized zone located at the glacier center

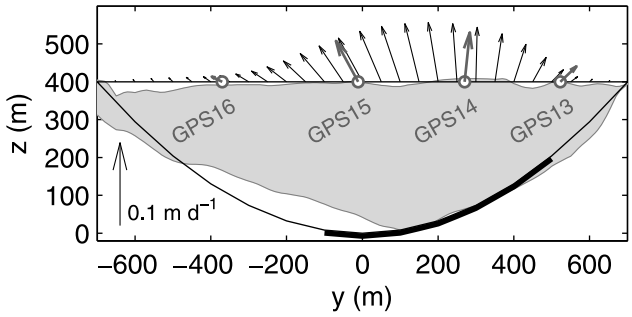

Figure 12. Surface flow vectors computed by Experiment 3 (black thin) and measured during the first half of Event 3 (June 11 0000 h–June 14 0000 h) (gray bold). Linear trends between the onset (June 11 0000 h) and the end (June 16 0000 h) of Event 3 are subtracted from the measured flow vectors. The bold line at the glacier bed indicates the location of the pressurized zone. The shaded area shows the actual glacier cross section along the GPS stations.

(Experiment 1: $y_0 = -100$ m, $y_1 = 100$ m, $\alpha = 1.138$). The vertical basal motion is transmitted to the surface and causes uplift in a region broader than the pressurized zone. The surface flow vectors have horizontal components of $u_y > 0$ at $y > 0$ and $u_y < 0$ at $y < 0$, resulting in ice motion toward the margins as observed in Gornergletscher. This result indicates that a locally elevated subglacial water pressure generates marginward ice motion as well as uplift on the glacier surface. When the pressurized zone is extended closer to the margins (Experiment 2: $y_0 = -500$ m, $y_1 = 500$ m, $\alpha = 1.0125$), the direction of the surface ice motion is more straight upward and the transverse motion is less significant near the glacier center (Figure 11c). The surface velocity distributions show transverse velocity peaks near the edges of the pressurized zone (Figure 11d). The peak locations are 100 m outside of the pressurized zone ($y = y_0 - 100$ m and $y_1 + 100$ m) in Experiment 1, yet 100 m inside ($y = y_0 + 100$ m and $y_1 - 100$ m) in Experiment 2. The magnitude of the transverse peak velocities are 33% of the maximum vertical velocity in Experiment 1 and 26% in Experiment 2.

[39] We repeated the experiment by changing the values of y_0, y_1, and α to obtain surface flow vectors similar to those observed during the first half of Event 3. A reasonable agreement with the observation was achieved by taking $y_0 = -100$ m, $y_1 = 500$ m, and $\alpha = 1.033$ (Experiment 3) as shown in Figure 12. The important features in the observation, such as nearly vertical motion at GPS14, marginward ice motion at GPS13 and GPS15, and relatively smaller motion at GPS16, were well reproduced by the model. The location of the pressurized zone prescribed in Experiment 3 is consistent with the discussion in the previous section. The model assumes that the flow path of the lake water is located in a region beneath GPS13–15, as suggested by the velocity change and uplift data (Figure 7) and the borehole water levels (Figure 8).

[40] A perfect agreement with the field data was not feasible since the assumed bottom boundary condition was too simple to simulate complex subglacial conditions. Moreover, the influence of the cold ice body was not considered and the elastic component in the ice mechanics was neglected in the model. Nevertheless, our experiments confirmed that the marginward motion occurs when the subglacial water pressure is locally elevated slightly above the ice overburden pressure.

[41] Another important aspect of the modeling results is the transmission of the ice motion from the bed to the surface. Such a problem has been investigated earlier for the transfer of basal sliding to horizontal surface motion [e.g., *Balise and Raymond*, 1985], but never studied for the basal separation and surface uplift. The flow vectors obtained by Experiments 1 and 2 clearly show that a greater portion of the vertical velocity is transferred to the surface when a broader pressurized zone is given (Figures 11b and 11c). The ratios of the surface to the basal vertical velocities at $y = 0$ are 0.36 and 1.07 for Experiments 1 and 2, respectively. Our numerical experiments indicate that the magnitude of surface uplift is not necessarily equal to the separation underneath the glacier, even if vertical strain of ice is negligible. Therefore, care should be taken when the magnitude of the basal separation is discussed from a point measurement on the surface. However, if the measurements are carried out at multiple locations across the glacier, spatial variations of the uplift and transverse motion can be used as a tool to estimate the location and magnitude of basal separation and distribution of subglacial water pressure.

6. Conclusion

[42] This study reports ice motion deviating toward the margins observed in Gornergletscher during three speed-up events in summer 2005. The high-frequency GPS measurements showed that the transverse velocity component increased as the glacier accelerated, resulting in ice motion toward the margins. The transverse ice motion reversed direction during the second half of each event, so that the survey stakes switched back to their original track. Four GPS receivers installed across the glacier revealed that the magnitude and the direction of the transverse velocity component were distributed systematically across the glacier. Our measurements also indicate that the transverse motion was correlated with surface uplift.

[43] Based on the detailed analysis of the transverse and vertical velocities, we propose the following mechanism for the marginward ice motion. When a limited part of the glacier bed is pressurized above the ice overburden pressure, the ice sole decouples from the bed and the vertical ice motion is transmitted from the bed to the surface. As the vertical basal motion propagates through the ice, transverse velocity components are generated, as also observed in ground motion during magma intrusion. The location of the subglacial drainage path estimated from the velocity change, uplift magnitude, and subglacial water pressure is consistent with this hypothesis.

[44] Numerical experiments with a two-dimensional ice flow model confirmed that the marginward ice motion occurs when the subglacial water pressure locally exceeds the ice overburden pressure. The measured surface flow vectors were well reproduced by tuning the location and magnitude of a high pressure zone at the bed. The location of the pressurized zone assumed in the model was in good agreement with the drainage path suggested by the surface speed and subglacial pressure measurements. Our observations and the modeling results reinforce our understanding

of glacier dynamics, and create a possibility to quantify the distributions of basal separation and subglacial water pressure from surface observations.

[45] **Acknowledgments.** We would like to thank the members of the field campaign at Gornergletscher in 2005. The lake-discharge data was provided by M. Huss. We are grateful to R. Greve and H. Blatter for insightful comments on the manuscript, and M. Truffer for helpful discussion. The paper was improved by careful reviews from D. Mair, R. S. Anderson, and an anonymous reviewer. S. Braun-Clarke and S. Hesse corrected the English. This research was funded by the Swiss National Science Foundation grant 200021-103882/1.

References

Amundson, J. M., M. Truffer, and M. P. Lüthi (2006), Time-dependent basal stress conditions beneath Black Rapids Glacier, Alaska, inferred from measurements of ice deformation and surface motion, *J. Glaciol.*, *52*(178), 347–357.

Anderson, R. S., S. P. Anderson, K. R. MacGregor, E. D. Waddington, S. O'Neel, C. A. Riihimaki, and M. G. Loso (2004), Strong feedbacks between hydrology and sliding of a small alpine glacier, *J. Geophys. Res.*, *109*, F03005, doi:10.1029/2004JF000120.

Balise, M. J., and C. F. Raymond (1985), Transfer of basal sliding variations to the surface of a linearly viscous glacier, *J. Glaciol.*, *31*(109), 308–318.

Bartholomaus, T. C., R. S. Anderson, and S. P. Anderson (2008), Response of glacier basal motion to transient water storage, *Nat. Geosci.*, *1*, 33–37.

Bauder, A., M. Funk, and M. Huss (2007), Ice volume changes of selected glaciers in the Swiss Alps since the end of the 19th century, *Ann. Glaciol.*, *46*, 145–149.

Bindschadler, R. (1983), The importance of pressurized subglacial water in separation and sliding at the glacier bed, *J. Glaciol.*, *29*(101), 3–19.

Eisen, O., A. Bauder, M. Lüthi, P. Riesen, and M. Funk (2009), Deducing the thermal structure in the tongue of Gornergletscher, Switzerland, from radar surveys and borehole measurements, *Ann. Glaciol.*, *50*, 63–70.

Glen, J. W. (1955), The creep of polycrystalline ice, *Proc. R. Soc. London, Ser. A*, *228*(1175), 519–538.

Gudmundsson, G. H. (1999), A three-dimensional numerical model of the confluence area of Unteraargletscher, Bernese Alps, Switzerland, *J. Glaciol.*, *45*(150), 219–230.

Gudmundsson, G. H. (2002), Observations of a reversal in vertical and horizontal strain-rate regime during a motion event on Unteraargletscher, Bernese Alps, Switzerland, *J. Glaciol.*, *48*(163), 566–574.

Gudmundsson, G. H., A. Bassi, M. Vonmoos, A. Bauder, U. H. Fischer, and M. Funk (2000), High-resolution measurements of spatial and temporal variations in surface velocities of Unteraargletscher, Bernese Alps, Switzerland, *Ann. Glaciol.*, *31*, 63–68.

Hooke, R. L., P. Calla, P. Holmlund, M. Nilsson, and A. Stroeven (1989), A 3 year record of seasonal variations in surface velocity, Storglaciären, Sweden, *J. Glaciol.*, *35*(120), 235–247.

Hubbard, A., H. Blatter, P. Nienow, D. Mair, and B. Hubbard (1998), Comparison of a three-dimensional model for glacier flow with field data from Haut Glacier d'Arolla, Switzerland, *J. Glaciol.*, *44*(147), 368–378.

Huss, M., A. Bauder, M. Werder, M. Funk, and R. Hock (2007), Glacier-dammed lake outburst events of Gornersee, Switzerland, *J. Glaciol.*, *53*(181), 189–200.

Iken, A., and R. A. Bindschadler (1986), Combined measurements of subglacial water pressure and surface velocity of Findelengletscher, Switzerland: Conclusions about drainage system and sliding mechanism, *J. Glaciol.*, *32*(110), 101–119.

Iken, A., H. Röthlisberger, A. Flotron, and W. Haeberli (1983), The uplift of Unteraargletscher at the beginning of the melt season—A consequence of water storage at the bed?, *J. Glaciol.*, *29*(101), 28–47.

Jansson, P. (1995), Water pressure and basal sliding on Storglaciären, northern Sweden, *J. Glaciol.*, *41*(138), 232–240.

Kamb, B., and H. Engelhardt (1987), Waves of accelerated motion in a glacier approaching surge: The mini-surges of Variegated Glacier, Alaska, U.S.A., *J. Glaciol.*, *33*(113), 27–46.

Magnússon, E., H. Rott, H. Björnsson, and F. Pálsson (2007), The impact of jökulhlaups on basal sliding observed by SAR interferometry on Vatnajökull, Iceland, *J. Glaciol.*, *53*(181), 232–240.

Mair, D., P. Nienow, I. Willis, and M. Sharp (2001), Spatial patterns of glacier dynamics during a high-velocity event: Haut Glacier d'Arolla, Switzerland, *J. Glaciol.*, *47*(156), 9–20.

Mair, D., M. Sharp, and I. Willis (2002), Evidence for basal cavity opening from analysis of surface uplift during a high-velocity event: Haut Glacier d'Arolla, Switzerland, *J. Glaciol.*, *48*(161), 208–216.

Mogi, K. (1958), Relations between the eruptions of various volcanoes and the deformations of the ground surfaces around them, *Bull. Earthquake Res. Inst. Univ. Tokyo*, *36*, 99–134.

Naruse, R., H. Fukami, and M. Aniya (1992), Short-term variations in flow velocity of Glacier Soler, Patagonia, Chile, *J. Glaciol.*, *38*(128), 152–156.

Nienow, P. W., M. J. Sharp, and I. C. Willis (1998), Seasonal changes in the morphology of the subglacial drainage system, Haut Glacier d'Arolla, Switzerland, *Earth Surf. Processes Landforms*, *23*, 825–843.

Nienow, P. W., A. L. Hubbard, B. P. Hubbard, D. M. Chandler, D. W. F. Mair, M. J. Sharp, and I. C. Willis (2005), Hydrological controls on diurnal ice flow variability in valley glaciers, *J. Geophys. Res.*, *110*, F04002, doi:10.1029/2003JF000112.

Pattyn, F., et al. (2008), Benchmark experiments for higher-order and full-Stokes ice sheet models (ISMIP-HOM), *Cryosphere*, *2*, 95–108.

Raymond, C. F., and S. Malone (1986), Propagating strain anomalies during mini-surges of Variegated Glacier, Alaska, U.S.A., *J. Glaciol.*, *32*(111), 178–191.

Riesen, P., T. Strozzi, A. Bauder, A. Wiesmann, and M. Funk (2009), Anomalous surface ice motion during the 2008 drainage of Gornersee, Switzerland, *Geophys. Res. Abstr.*, *11*, EGU2009-11362-1.

Röthlisberger, H., and A. Iken (1981), Plucking as an effect of water-pressure variations at the glacier bed, *Ann. Glaciol.*, *2*, 57–61.

Ryser, C. (2008), The polythermal structure of Grenzgletscher, Valais, Switzerland, Master's thesis, Lab. of Hydraul. Hydrol. and Glaciol., ETH Zurich, Zurich, Switzerland.

Sugiyama, S., and G. H. Gudmundsson (2003), Diurnal variations in vertical strain observed in a temperate valley glacier, *Geophys. Res. Lett.*, *30*(2), 1090, doi:10.1029/2002GL016160.

Sugiyama, S., and G. H. Gudmundsson (2004), Short-term variations in glacier flow controlled by subglacial water pressure at Lauteraargletscher, Bernese Alps, Switzerland, *J. Glaciol.*, *50*(170), 353–362.

Sugiyama, S., G. H. Gudmundsson, and J. Helbing (2003), Numerical investigation of the effects of temporal variations in basal lubrication on englacial strain-rate distribution, *Ann. Glaciol.*, *37*, 49–54.

Sugiyama, S., A. Bauder, P. Weiss, and M. Funk (2007), Reversal of ice motion during the outburst of a glacier-dammed lake on Gornergletscher, Switzerland, *J. Glaciol.*, *53*(181), 172–180.

Sugiyama, S., A. Bauder, M. Huss, P. Riesen, and M. Funk (2008), Triggering and drainage mechanisms of the 2004 glacier-dammed lake outburst in Gornergletscher, Switzerland, *J. Geophys. Res.*, *113*, F04019, doi:10.1029/2007JF000920.

Truffer, M., K. Echelmeyer, and W. D. Harrison (2001), Implications of till deformation on glacier dynamics, *J. Glaciol.*, *47*(156), 123–134.

Vieli, A., J. Jania, H. Blatter, and M. Funk (2004), Short-term velocity variations on Hansbreen, a tidewater glacier in Spitsbergen, *J. Glaciol.*, *50*(170), 389–398.

Walsh, J. B., and R. W. Decker (1971), Surface deformation associated with volcanism, *J. Geophys. Res.*, *76*(14), 3291–3302.

Walter, F., N. Deichmann, and M. Funk (2008), Basal icequakes during changing subglacial water pressures beneath Gornergletscher, Switzerland, *J. Glaciol.*, *54*(186), 511–521.

Werder, M., and M. Funk (2009), Dye tracing a jökulhlaup: II. Testing a jökulhlaup model against flow speeds inferred from measurements, *J. Glaciol.*, *55*(193), 899–908.

Werder, M., A. Loye, and M. Funk (2009), Dye tracing a jökulhlaup: I. Subglacial water transit speed and water-storage mechanism, *J. Glaciol.*, *55*(193), 889–898.

Zwally, H. J., W. Abdalati, T. Herring, K. Larson, J. Saba, and K. Steffen (2002), Surface melt-induced acceleration of Greenland ice-sheet flow, *Science*, *297*(5579), 218–222.

A. Bauder, M. Funk, and P. Riesen, Laboratory of Hydraulics, Hydrology and Glaciology, ETH Zurich, Gloriastrasse 37/39, CH-8092 Zurich, Switzerland. (bauder@vaw.baug.ethz.ch; funk@vaw.baug.ethz.ch; riesen@vaw.baug.ethz.ch)

S. Sugiyama, Institute of Low Temperature Science, Hokkaido University, Nishi-8, Kita-19, Sapporo, 060-0819, Japan. (sugishin@lowtem.hokudai.ac.jp)